Inhibition of both focal adhesion kinase and insulin-like growth factor-I receptor kinase suppresses glioma proliferation *in vitro* and *in vivo*

Ta-Jen Liu,[1,3] Tiffany LaFortune,[1] Toshiyuki Honda,[3] Osamu Ohmori,[3] Shinji Hatakeyama,[3] Thomas Meyer,[4] Dowdy Jackson,[5] John de Groot,[1] and W.K. Alfred Yung[1]

[1]Brain Tumor Center, Department of Neuro-Oncology, The University of Texas M. D. Anderson Cancer Center; [2]Graduate School of Biomedical Sciences, The University of Texas-Houston Health Science Center, Houston, Texas; [3]Lab. Head of Discovery Biology, Novartis Institutes for BioMedical Research, Tsukuba, Ibaraki, Japan; [4]Expertise Program Kinases, Novartis Institutes for BioMedical Research, Basel, Switzerland; and [5]MedImmune, Inc., Gaithersburg, Maryland

Abstract

Multiple genetic aberrations in human gliomas contribute to their highly infiltrative and rapid growth characteristics. Focal adhesion kinase (FAK) regulates tumor migration and invasion. Insulin-like growth factor-I receptor (IGF-IR), whose expression correlates with tumor grade, is involved in proliferation and survival. We hypothesized that inhibiting the phosphorylation of FAK and IGF-IR by NVP-TAE226 (hereafter called TAE226), a novel dual tyrosine kinase inhibitor of FAK and IGF-IR, would suppress the growth and invasion of glioma cells. In culture, TAE226 inhibited extracellular matrix–induced autophosphorylation of FAK (Tyr^{397}). TAE226 also inhibited IGF-I–induced phosphorylation of IGF-IR and activity of its downstream target genes such as *MAPK* and *Akt*. TAE226 retarded tumor cell growth as assessed by a cell viability assay and attenuated G_2-M cell cycle progression associated with a decrease in cyclin B1 and phosphorylated cdc2 (Tyr^{15}) protein expression. TAE226 treatment inhibited tumor cell invasion by at least 50% compared with the control in an *in vitro* Matrigel invasion assay. Interestingly, TAE226 treatment of tumor cells containing wild-type p53 mainly exhibited G_2-M arrest, whereas tumor cells bearing mutant p53 underwent apoptosis. Induction of apoptosis by TAE226 was substantiated by detection of caspase-3/7 activation and poly(ADP-ribose) polymerase cleavage and by an Annexin V apoptosis assay. More importantly, TAE226 treatment significantly increased the survival rate of animals in an intracranial glioma xenograft model. Collectively, these data show that blocking the signaling pathways of FAK and IGF-IR with TAE226 has the potential to be an efficacious treatment for human gliomas. [Mol Cancer Ther 2007;6(4):1357–67]

Introduction

Gliomas are the third most frequent cause of cancer-related deaths in adults and the second most in children (1). Glioblastomas, the most malignant form of primary gliomas, are characterized by high infiltration of surrounding normal brain without metastasis to distant sites. Despite numerous advances in chemotherapeutic, radiation, and surgical procedures, the survival rate for patients with gliomas/glioblastomas has essentially remained unchanged for the past 30 years. Even when different treatment regiments are combined, resistant tumor cells infiltrate normal brain tissue, so that tumor recurrence is inevitable. Because tumor invasion into the local environment is an important factor in the morbidity and mortality of cancer patients with brain tumors, development of novel therapeutic strategies or agents that disrupt tumor invasion will be beneficial to patients with glioma.

Neoplastic transformation in the normal human brain occurs as a result of the accumulation of a series of genetic alterations. These genetic alterations include the loss, gain, or amplification of different chromosomes, which lead to altered expression of proteins that play important roles in the regulation of cell proliferation. For example, focal adhesion kinase (FAK), a non–receptor-type tyrosine kinase, is expressed in most tumor and normal cells and is required for cell proliferation, migration, and survival (2). A handful of studies have shown the association between FAK and grade of malignancy (3), vascularity (4), and proliferation and migration of gliomas (5). FAK can be activated upon ligand binding and clustering of integrin receptors as well as activation of other cell surface receptors such as epidermal growth factor receptor (EGFR; ref. 6). Integrin family binding of transmembrane receptors with the extracellular matrix induces recruitment of FAK from the cytoplasm, which stimulates autophosphorylation of FAK at its Tyr^{397} residue. This mechanism makes SH2-binding sites available for the recruitment of Src family tyrosine kinase(s). Further phosphorylation of FAK creates binding sites for growth factor receptor binding protein 2 and Cas adaptor and docking proteins. Similar to the cytoplasmic domain of a receptor tyrosine kinase, FAK

Received 8/8/06; revised 12/7/06; accepted 2/26/07.

Grant support: Commonwealth Cancer Foundation and M. D. Anderson Cancer Center Support grant CA16672.

The costs of publication of this article were defrayed in part by the payment of page charges. This article must therefore be hereby marked *advertisement* in accordance with 18 U.S.C. Section 1734 solely to indicate this fact.

Requests for reprints: Ta-Jen Liu, Department of Neuro-Oncology, The University of Texas M. D. Anderson Cancer Center, Unit 1002, 1515 Holcombe Boulevard, Houston, TX 77030. Phone: 713-834-6203; Fax: 713-834-6230. E-mail: tjliu@mdanderson.org

doi:10.1158/1535-7163.MCT-06-0476

functions as both a kinase and docking protein in these complexes. Therefore, FAK participates in multiple cell functions required for cell proliferation, survival, motility, and invasion (7, 8). Experiments designed to disrupt FAK signaling, such as overexpressing a kinase-dead FAK mutant (FRNK; ref. 9) or a small interfering RNA–induced silencing of the expression of FAK (10), resulted in antiproliferative activity. These observations suggest that FAK inactivation could be a potential targeted therapy for treatment of gliomas.

The insulin-like growth factor-I receptor (IGF-IR) has been shown to play a role in growth and proliferation of many tumor types. It is a transmembrane receptor tyrosine kinase, which is primarily activated by IGF-I and IGF-II. The activated IGF-IR signaling pathway either through high levels of IGF-IR and/or its ligands IGF-I and IGF-II has been associated with various types of human cancers including gliomas and medulloblastomas (11, 12). This high level of expression has also been correlated with increased tumor cell invasiveness and metastatic potential (13–15). IGF-IR signaling cascades activate both Akt and mitogen-activated protein kinase (MAPK) and has been shown to protect cancer cells from apoptosis induced by various anticancer drugs and radiation (16, 17). In the central nervous system, IGF-IR has been implicated in fetal and postnatal growth and development of the brain (18) as well as in brain tumorigenesis. The presence of an active IGF system has been shown in astrocytomas (12) and glioblastomas (19). These findings strongly indicate that the IGF-IR signaling pathway might contribute to the highly infiltrative characteristic of gliomas. Inhibiting the IGF-IR signaling pathway by blocking its expression via antisense (19, 20), by preventing ligand binding with an antibody (21), or by blocking its signaling capacity with a dominant-negative form of the receptor (22) has been shown to reduce tumor progression and/or metastasis formation in animal models.

In the present study, we investigated the antitumor activity of a novel compound TAE226, a potent ATP-competitive inhibitor of several tyrosine protein kinases, in particular FAK and IGF-IR kinases. In a cell-based kinase assays, FAK, IGF-IR kinase, and IR kinase were inhibited with an IC_{50} range of 100 to 300 nmol/L compared with the other kinases tested, which were >10-fold less sensitive. We show that TAE226 antagonized both FAK and IGF-IR signaling pathways, resulting in growth inhibition, cell cycle arrest, attenuation of tumor invasion, and induction of apoptosis. More importantly, TAE226 significantly prolonged the survival of animals bearing intracranial glioma xenografts, showing the potential therapeutic efficacy of using TAE226 to treat patients with glioblastomas.

Materials and Methods

Cell Lines and Culture Conditions

To assess the levels of IGF-IR and FAK in human gliomas as well as the effect of TAE226, we used the following cell lines: U87, U87/EGFR (U87 cells stably expressed wild-type EGFR [wt-EGFR]; ref. 23), U87/vIII (U87 cells stably expressed EGFR variant III [EGFRvIII] mutant; ref. 23), U251, U251/EGFR (U251 stably expressed wt-EGFR; ref. 24), U373, LN229, LN382T, LN18, LN308, A172, D54, SNB19, U343 (25). Cell lines expressing wild-type p53 (wt-p53) used in the detailed study were D54, U343, U87, and U87 isogenic cell lines. Cell lines bearing mutant-p53 used in the detailed study were U251, LN18, and LN229. All cell lines were maintained as monolayer cultures in DMEM/F12 supplemented with 10% fetal bovine serum and penicillin/streptomycin (all from Life Technologies, Inc., Grand Island, NY). Cell cultures were maintained and incubated as described previously (26).

Reagents

NVP-TAE226 was synthesized and generously provided by Novartis Pharma AG (Basel, Switzerland) through a material transfer agreement with the University of Texas M.D. Anderson Cancer Center. For use *in vitro*, TAE226 was dissolved in DMSO (Sigma-Aldrich Corp., St. Louis, MO) to a concentration of 10 mmol/L, stored at −20°C, and further diluted to an appropriate final concentration in DMEM. DMSO in the final solution did not exceed 0.1% (v/v).

Measurement of Cell Proliferation

The antiproliferative activity of TAE226 on cells growing in culture was determined using a tetrazolium-based colorimetric [3-(4,5-dimethylthiazol-2-yl)-2,5-diphenyltetrazolium bromide] assay as described previously (24).

Cell Viability Assay

Cell cultures were harvested with 0.05% trypsin and seeded in triplicate at 2×10^4 in 24-well culture plates for 24 h before drug treatment. Culture medium was used for mock treatment. Cells were harvested at the indicated day after treatment, and viable cells were counted using the Vi-cell viability analyzer.

Cell Invasion Assay

Invasion of glioma cells *in vitro* was measured by the invasion of cells through Matrigel-coated 12-well Boyden inserts as described previously (27). Quantification of invasion was done by dissolving the inserts in 2% deoxycholate solution and measuring the absorbance at 595 nm.

Gelatin Substrate Zymography

Glioma cells culture treated with TAE226 for 48 h were replaced with fresh serum-free medium for an additional 24 h. Conditioned medium was collected and concentrated with equal volumes of ethanol, resuspended in radioimmunoprecipitation assay buffer, and subjected to analysis as described previously (27).

Immunofluorescence Staining

Glioma cells were plated on a six-well culture plate at 2×10^4 per well for 24 h and subsequently treated with TAE226 for 48 h. Thereafter, the cells were fixed with 4% paraformaldehyde in PBS for 20 min and then permeabilized with 1.0% Triton X-100 in PBS for 5 min. Tubulin was visualized by incubating first with mouse anti-α-tubulin monoclonal antibody and then with Texas red–conjugated goat antibody to mouse IgG. Filamentous-actin filaments were stained with phalloidin conjugated with Alexa Fluor

488 (Invitrogen, Carlsbad, CA). Nuclei were stained with 1 μg/mL Hoescht 33258 for 10 min at room temperature. Pictures were taken under a Zeiss Axioskop 40 microscope equipped with appropriate filters with aid of Axio Vision 4.4 software.

Cell Cycle Analysis

Glioma cells were plated at a density of 3×10^5 per well in 60-mm plates (Costar, Cambridge, MA) and maintained in 10% fetal bovine serum medium overnight. The next day, the cells were washed twice and maintained in 10% fetal bovine serum medium before treatment with TAE226 and subjected to flow cytometric analysis as described previously (26).

Western Blotting Analysis

To determine whether TAE226 acted through its purported mechanism *in vitro*, we evaluated the effect of this agent on inhibition of IGF-I–stimulated tyrosine phosphorylation of IGF-IR, MAPK, and AKT in human U87 and U251 glioma cells. Under basal conditions in serum-free media, both cells showed a low level of autophosphorylation, which was enhanced after exposure to IGF-I for 30 min. These cell lines were plated onto 10-cm plates at a concentration of 5×10^5 per plate and then incubated for 24 h. On the next day, cells were incubated with serum-free media for 24 h with various concentrations of TAE226, ranging from 0.25 to 1 μmol/L, and controls. The cells were then activated with recombinant IGF-I (100 ng/mL) for 30 min. The membrane was probed with primary antibodies. Primary antibodies used in this study were IGF-IRα, IGF-IRβ, phosphorylated IGF-IR (p-IGF-IR; $Tyr^{1135/1136}$), p-Akt (Ser^{473}), p-MAPK (Thr^{202}/Tyr^{204}), total FAK, total MAPK, cleaved caspase-3 (Asp^{175}), caspase-7 (Asp^{198}), poly(ADP-ribose) polymerase (PARP), Bax, cdc2, p-cdc2, and cyclin B1 (Cell Signaling, Boston, MA). P-FAK (pY397) was purchased from Biosource International (Camarillo, CA). Anti-β-actin antibody was purchased from Sigma-Aldrich.

Apoptosis Assay

Apoptosis was quantified using the Annexin V-FLUOS Apoptosis kit (Roche, Indianapolis, IN) according to the manufacturer's instructions. U87, D54, U343, U251, and LN18 glioma cells were continuously incubated in drug for 72 h before subjected to the flow cytometric analysis.

Intracranial Animal Model Study

Male nude mice were purchased from the National Cancer Institute-Frederick Cancer Research and Development Center (Frederick, MD). Mice were maintained in a pathogen-free environment and used in accordance with the Animal Care and Use Guidelines of the University of Texas M.D. Anderson Cancer Center. Mice used for this study were 6 to 8 weeks old. In DMEM/F12 serum-free media (5 μL), 5×10^5 of U87 cells and 1×10^6 of LN229 cells per mouse were implanted intracranially through a guide-screw system as described previously (28). Four days after injection of the tumor cells, mice were randomized into three groups for each cell line ($n = 6$). Mice in group 1 were treated with 50 mg/kg TAE226 in 200 μL of 0.5% methylcellulose, via an oral gavage. The mice in group 2 received 75 mg/kg TAE226 in 200 μL of 0.5% methylcellulose. The mice in group 3 the same vehicle used for administration of TAE226 (control). Treatment frequency was once a day for 5 days and off for 2 days, for a duration of 4 weeks. Mice were monitored daily. Mice were euthanized when they were moribund, and the whole brain was extracted for rapid freezing in liquid nitrogen and storage at −70°C.

Statistical Analyses

For the *in vitro* experiments, statistical analyses were done using a two-tailed Student's *t* test. Data are mean ± SD. The *in vivo* therapeutic efficacy of TAE226 was assessed by plotting survival curves according to the Kaplan-Meier method, and groups were compared using the log-rank test.

Results

TAE226 Inhibits Extracellular Matrix–Induced FAK and IGF-I–Induced IGF-IR Phosphorylation and Blocks Activation of Downstream Target Genes

The potency and selectivity of NVP-TAE226 was assessed in *in vitro* kinase assays with several recombinant kinase domains and peptide substrates (Table 1). NVP-TAE226 inhibited the recombinant FAK kinase domain with an IC_{50} of 0.0055 μmol/L and was equipotent against the recombinant proline-rich tyrosine kinase 2 domain. NVP-TAE226 was ~10- to 100-fold less potent against IR, IGF-IR, ALK, and c-Met kinases and >100-fold less potent against the remaining kinases tested.

Endogenous levels of FAK and IGF-IR were assessed in a battery of glioma cell lines. It has been shown that the FAK signaling pathway is activated by signaling of growth factor receptors such as EGFR (6). Isogenic cell lines of U87 and U251 expressing either wt-EGFR or EGFRvIII were therefore included in the analysis for detection of FAK levels. Results from Western blotting analyses showed that glioma cell lines express different levels of p-FAK (Tyr^{397}), an index of FAK activity (Fig. 1A). Protein extract from 293 cells transiently transfected with a FAK expression vector was used as a positive control for size determination of FAK. Of interest, among U87 isogenic cell lines, it seemed that EGFRvIII expression resulted in the highest p-FAK levels followed by wt-EGFR and the parental cells. It is not surprising because EGFRvIII-expressing cells possessed constitutive tyrosine kinase activity in the absence of EGF ligand, whereas the tyrosine kinase activity in the wt-EGFR–expressing cells required ligand stimulation (23). The expression of both IGF-IRα (130 kDa) and IGF-IRβ subunits (90 kDa) also varied among the different cell lines (Fig. 1B).

The signaling events that are evoked immediately upon integrin ligation and attachment of cells to extracellular matrix have been described (29). Engaging integrins in this manner activates FAK by augmenting phosphorylation at its Tyr^{397} residue. Accordingly, we wanted to determine if TAE226 treatment abrogates integrin-induced FAK autophosphorylation. As shown in Fig. 2A, the level of p-FAK (Tyr^{397}) was induced by 1.5-fold in U87 and 1.8-fold in

Table 1. ***In vitro*** **(purified enzyme) inhibition profile of TAE226**

Enzyme	IC_{50} (μmol/L)	SD	*n*	Type of kinase
FAK	0.0055	0.00053	4	Tyr
Pyk2	(0.005, 0.002)		2	Tyr
c-Src	(0.92, 0.89)		2	Tyr
c-Abl	(6.9, 4.8)		2	Tyr
HER-1	1.7		1	Tyr
HER-2	(0.98, 0.91)		2	Tyr
c-Met	0.16	0.17	4	Tyr
KDR	0.36	0.23	6	Tyr
Flt1	3.4	1.05	3	Tyr
Flt3	0.48		1	Tyr
Flt4	0.22		1	Tyr
FGFR1	0.75	0.35	4	Tyr
FGFR3/K650E	0.63		1	Tyr
c-Kit	(>10, 1.8)		2	Tyr
PDGFR-β	2.6	1.60	5	Tyr
Tek	0.58	0.16	3	Tyr
IGF-IR	(0.16, 0.12)		2	Tyr
Ins-R	(0.026, 0.061)		2	Tyr
Ret	1.3		1	Tyr
Ret M918T	2.3		1	Tyr
JAK-2	0.84		1	Tyr
Lck	(>10, 7.1, >10)		3	Tyr
Syk	7.9	3.0	4	Tyr
ZAP-70	7.7	3.5	4	Tyr
CDK1/cyclin B	0.54	0.038	3	Ser/Thr
PKA	>10.0		3	Ser/Thr
PKB/AKT	>10.0		3	Ser/Thr
PDK1	2.4		1	Ser/Thr
c-Raf	>10.0		3	Ser/Thr

NOTE: The potency and selectivity of TAE226 was assessed in *in vitro* kinases with several recombinant kinase domains and peptide substrates. Mean IC_{50} was shown with SD when assays were done more than twice ($n \geq 3$).

Abbreviations: Tyr, protein tyrosine kinase; Ser/Thr, protein serine/threonine kinase; Pyk2, proline-rich tyrosine kinase 2; HER, human EGFR; Met, hepatocyte growth factor receptor; KDR, kinase domain receptor; Flt, Fms-like tyrosine kinase; FGFR, fibroblast growth factor receptor; Kit, stem cell factor receptor; PDGFR, platelet-derived growth factor receptor; Tek, angiopoietin 1/2 receptor/Tie2; Ret, receptor tyrosine kinase; JAK, janus-activated kinase; Lck, lymphoid T-cell protein tyrosine kinase; ZAP-70, zeta chain-associated protein of 70 kDa; CDK, cyclin-dependent kinase; PKA, protein kinase A; PKB, protein kinase B; PDK, phosphoinositide-dependent protein kinase.

U251 cell line on collagen-coated plates compared with uncoated control (Fig. 2B). A concentration of 0.25 μmol/L TAE226, which is smaller than 1 μmol/L [the IC_{50} concentration established by a 3-(4,5-dimethylthiazol-2-yl)-2,5-diphenyltetrazolium bromide assay; data not shown], effectively inhibited collagen-stimulated p-FAK (Tyr^{397}) expression. Interestingly, an obvious dose-dependent inhibition of TAE226 on FAK activity was noted in U87 but not in U251 cell line (Fig. 2B) possibly due to the level of integrin in U251 that might require higher concentration of TAE226 to antagonize the FAK activity.

To determine whether TAE226 could inhibit IGF-I-stimulated signaling pathways, U87 and U251 glioma cell lines were serum depleted and incubated in the presence or absence of various concentrations of TAE for 24 h. Cells were then stimulated with or without 100 ng/mL IGF-I for 30 min. Cellular extracts were then assessed by Western blotting analysis to determine the expression of p-IGF-IR and total IGF-IRβ, Akt, and MAPK protein. Upon binding of its ligands, phosphorylation of the triple tyrosine cluster (Tyr^{1131}, Tyr^{1135}, and Tyr^{1136}) within the kinase domain is the earliest major site of autophosphorylation (30). P-IGF-IRβ ($Tyr^{1135/1136}$) was significantly induced by IGF-I more so in U251 cells than in U87 cells (Fig. 2C) likely due to the difference in IGF-IR expression between the two cell lines (Fig. 1B). Such an induction was reduced to and lower than the baseline of the untreated and unstimulated control levels by 0.25 μmol/L TAE226 in U251 and U87, respectively. Activity of two notable downstream target genes in the IGF-IR signaling pathway (*Akt* and *MAPK*) were also inhibited by TAE226 as assessed by the decrease in expression of p-Akt (Ser^{473}) and p-MAPK (Thr^{202}/Tyr^{204}) levels. Total levels of IGF-IRβ, MAPK, and Akt were also determined (Fig. 2C). Quantitative analysis of the effect of TAE226 on both Akt and MAPK activities shown in Fig. 2D showed that TAE226 was able to effectively antagonize the kinase activity of FAK and IGF-IR, subsequently inactivating the downstream target genes *Akt* and *MAPK*. Cells

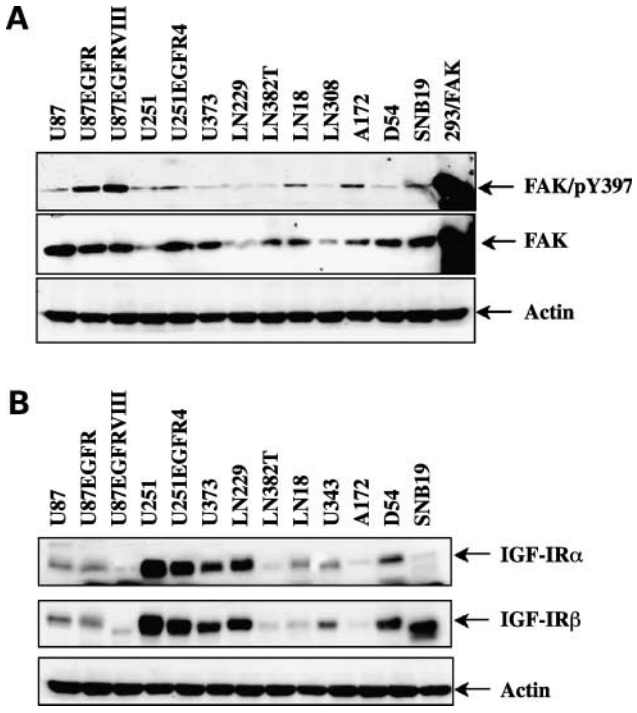

Figure 1. Expression profiles of FAK and IGF-IR in glioma cell lines. **A,** a battery of glioma cell lines was assessed for their expression of autophosphorylated and total FAK by Western blot analysis using anti–phospho-FAK (Tyr^{397}) and anti-FAK, respectively. Extract from 293 cells transiently transfected with a FAK expression plasmid was used as control for determining the size of FAK. **B,** expression of IGF-IRα and IGF-IRβ subunits was examined in the same protein extracts as separate blots using anti-IGF-IRα and anti-IGF-IRβ. Expression of β-actin was used as a loading control.

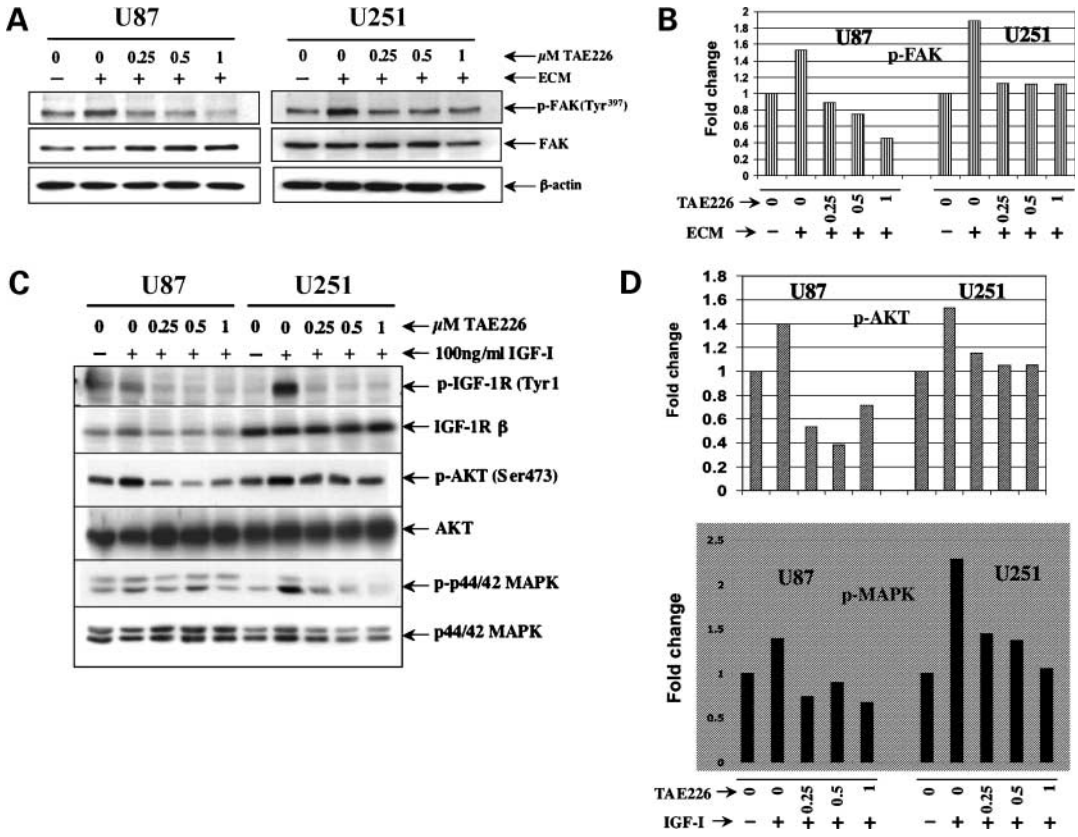

Figure 2. TAE226 treatment inhibits FAK and IGF-IR signaling pathways. **A,** serum-starved glioma cells were seeded on a Vitrogen-coated plate (20 μg/mL) for 2 h before different concentrations of TAE226 were added for 4 h. Cell extracts were then harvested for Western blotting analysis to detect the autophosphorylated form of FAK (Tyr^{397}). TAE226 inhibited the extracellular matrix (*ECM*) – induced activation of FAK. Expression of β-actin was used as a loading control. **B,** quantitative analysis of the dose effect of TAE226 on extracellular matrix – induced p-FAK after normalization with total FAK expression in each experiment. The fold change of p-FAK and total FAK from the uninduced and untreated sample was arbitrarily set as 1. **C,** cells on a six-well culture plate were serum-depleted for 24 h before they were treated without or with various concentrations of TAE226 along with 100 ng/mL IGF-I for an additional 30 min. Cell extracts were harvested and subjected to Western blotting analysis for the detection of p-IGF-IRβ ($Tyr^{1135/1136}$). Expression of IGF-IR downstream target genes, such as *AKT* and *MAPK*, was also examined. TAE226 inhibited the ligand-induced IGF-IR signaling pathway. **D,** quantitative analysis of the effect of TAE226 treatment on IGF-I – induced p-AKT and p-MAPK (*shaded graph*) activities in one representative Western blot. Densitometry was done using NIH Image J software.

treated with media containing 1% of vehicle (DMSO) did not affect signaling or viability (data not shown); therefore, vehicle control was substituted with media control throughout the investigation.

TAE226 Treatment Inhibits Glioma Cell Growth and Disrupts Glioma Cell Cycle Progression

To explore the antitumor activity of TAE226 on glioma cell lines and determine if FAK and IGF-IR expression correlates with sensitivity to TAE226 treatment, we chose four cell lines expressing different level of FAK and IGF-IR, as shown in Fig. 1A. U87, U87/EGFR, and U87/EGFRvIII cell lines were parental cells, cells stably expressing EGFR, and cells stably expressing the EGFRvIII mutant (23), respectively. The U251 cell line expressed the lowest level of FAK but highest level of IGF-IR. Cell lines were treated with different concentrations of TAE226 (1 and 10 μmol/L), and viable cells were counted at days 1, 3, and 5 after treatment using a trypan blue exclusion method. The effect of TAE226 on tumor cell growth is shown in Fig. 3A. TAE226 treatment significantly retarded the growth of all cell lines tested in a concentration-dependent manner, albeit having no direct correlation between FAK and IGF-IR expression and sensitivity to TAE226 treatment. However, comparisons among the different U87 cell lines suggested that U87/EGFR and U87/EGFRvIII cell lines, which express a higher level of p-FAK (Tyr^{397}) than parental U87 (Fig. 1A), were more sensitive to TAE226. Day 5 after TAE226 treatment, there were 22%, 14%, and 17% of viable U87, U87/EGFR, and U87/EGFRvIII cells over their untreated control, respectively. Interestingly, in addition to their flat, enlarged morphology, resembling cellular senescence (31, 32), TAE226-treated cells became multinucleated, which suggested that TAE226 may disrupt cell cycle progression (Fig. 3B). Moreover, in comparison with U87 cells, prolonged incubation of U251 cells with TAE226 generated floating cells with the appearance of membrane blebs, echoing the apoptotic process (ref. 33; data not shown). These observations raised an intriguing possibility

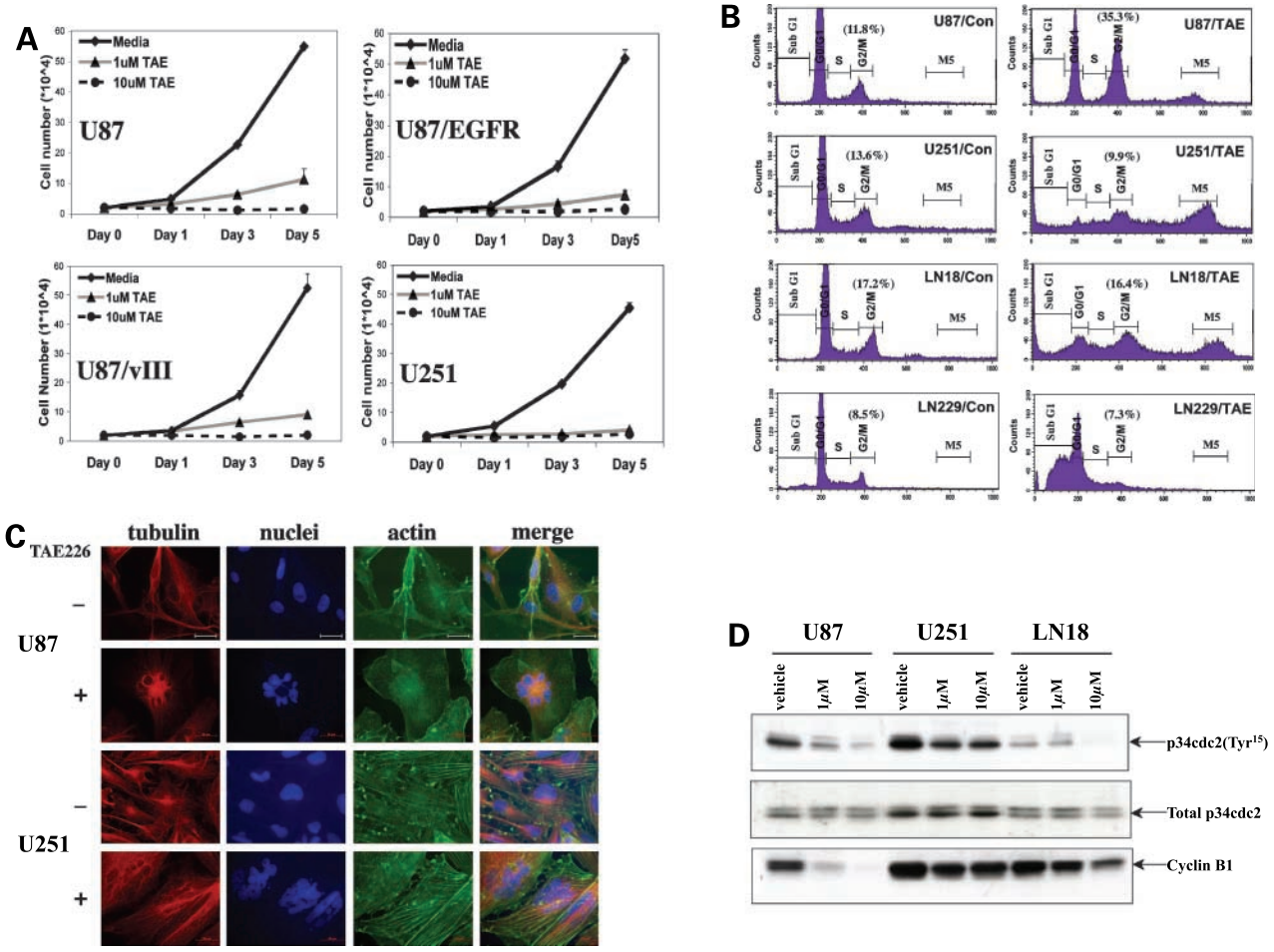

Figure 3. TAE226 treatment inhibits glioma cell growth and disrupts cell cycle distribution. **A,** cells were plated at 2×10^4 per well in a 24-well culture dish. At day 0, cells were treated with 1 and 10 μmol/L TAE226 along with a vehicle treatment control. Cells were trypsinized on days 1, 3, and 5 after TAE226 treatment, and viable cells were scored using a Beckman Coulter Vi-cell viability analyzer. *Points,* mean of triplicate samples; *bars,* SD. **B,** cell cycle analysis was done on cells treated or untreated with 1 μmol/L TAE226 for 48 h. Cell cycle distribution was labeled on the histogram. M5 fraction represents tetraploid cells with DNA content ≥ 8N. **C,** immunofluorescence staining of both U87 and U251 cells following 1 μmol/L TAE226 treatment for 48 h. Tubulin structure was visualized using anti-α-tubulin and Texas red–conjugated goat anti-mouse antibodies. Nuclei were stained with Hoescht 33258. Organization of filamentous actin was detected after staining with Alexa Fluor 488–conjugated phalloidin. Pictures were taken using a Zeiss microscope equipped with appropriate filters. TAE226-treated cells exhibited enlarged cells with multiple nuclei (×60). Bar, 20 μm. **D,** effect of TAE226 on the expression of mitosis initiators p34cdc2 and cyclin B1. P-p34cdc2 (Tyr^{15}) levels decreased in TAE226-treated cell lines, whereas total p34cdc2 levels remained unchanged. TAE226 treatment also decreased the level of cyclin B1.

that TAE226 treatment might induce apoptosis correlating with p53 status in tumor cells because the U87 cell line contains the *wt-p53* gene, whereas U251 cell line possesses the mutant p53 (*mut-p53*) gene.

We examined the effect of TAE226 on glioma cell cycle distribution, in particular the sub-G_1 population indicative of apoptosis using flow cytometric analysis. Three glioma cell lines containing mut-p53 (U251, LN18, and LN229) and one with wt-p53 (U87) were used for the investigation. Glioma cells were treated either with or without 1 μmol/L TAE for 48 h before harvesting for cell cycle analysis. When the U87 glioma cell line was exposed to TAE226, the number of cells in G_2-M increased from 7.0% to 35.3%, whereas cells in G_0-G_1 were markedly decreased from 77.4% to 32.8% compared with the controls. The percentage of cells in sub-G_1 was minimally affected by TAE226 treatment (1.2-fold increase over control). In sharp contrast, sub-G_1 population of U251, LN18, and LN229 cell lines following TAE226 treatment showed a 4.8-fold, 12.8-fold, and 13.0-fold increase, respectively, as shown in Fig. 3B. The population of cells in the G_2-M phase was similar between the treated and untreated in these three mut-p53 cell lines.

Interestingly, the M5 cell population with an 8N DNA content increased significantly in all treated cell lines, suggesting that TAE226 induced the formation of tetraploid cells (Fig. 3B). These observations were further confirmed by immunofluorescence staining of cell nuclei with Hoescht 33258. TAE226-treated cells became multinucleated compared with untreated cells with single nuclear staining

(Fig. 3C). The size of the nuclei and the number of giant cells increased as much as 3-fold in the presence of the drug compared with controls. The microtubule network was examined after staining with α-tubulin, showing that the intracellular microtubule network extends throughout the cytoplasm in both TAE226-treated and untreated cells. When TAE226-treated cells were stained, multiple nuclei were found in single tubulin-surrounded cells. The cytoskeletal network was visualized by staining stress actin with Alexa Fluor 448–conjugated phalloidin.

Because these results suggest that TAE226 disrupts G_2-M progression, we examined the expression of proteins that control the G_2-M cell cycle checkpoint. For cells to enter mitosis, the mitosis initiator MPF (cdc2/cyclin B1) has to be properly regulated, accompanied by the dephosphorylation of p34cdc2 kinase on Tyr^{15} (34). It has been shown that depletion of cyclin B1 with small interfering RNA resulted in G_2-M cell cycle arrest and, subsequently, induction of apoptosis (35). In our experiments, TAE226 treatment of glioma cell lines reduced the expression of p-cdc2 (Tyr^{15}) and cyclin B1 in a dosage-dependent manner (Fig. 3D). These results indicate that TAE226-induced G_2-M phase cell cycle arrest in glioma cells is associated with a marked decline in cyclin B1 and p-cdc2 protein expression.

TAE226 Treatment Inhibits Glioma Cell Invasion

Because FAK is instrumental in cell motility, and because IGF-IR plays an important role in tumor invasion, we wanted to determine if TAE226 affects glioma cell invasion. Glioma cell lines U87, U87/EGFRvIII, U251, and LN18 were treated with or without 1 μmol/L TAE226 for 24 h before subjected to an *in vitro* Matrigel invasion assay. The results shown in Fig. 4A (*top*) showed that treatment with TAE226 significantly decreased the invasive propensity of glioma cells. Quantification (Fig. 4B) of these results showed that TAE226 treatment inhibits glioma cell invasion by at least 50% of untreated control.

Matrix metalloproteases (MMP), in particular MMP-2 and MMP-9, degrading extracellular matrix components have been implicated in glioma invasion. We examined if inhibiting tumor invasion *in vitro* was associated with reduced MMP-2 activity. Serum-free conditioned media collected from 1 μmol/L TAE226–treated or untreated cells were subjected to a gelatin zymographic analysis. Results in Fig. 4C showed that MMP-2 enzymatic activity in TAE226-treated cells was similar to untreated cells, suggesting that TAE226 inhibition of glioma cell invasion is likely due to affect motility.

TAE226 Treatment Induces Apoptosis in Glioma Cells Containing mut-p53

Cell cycle analysis showed that TAE226 was responsible for an elevated sub-G_1 population in U251, LN18, and LN229 but not in U87, suggesting that TAE226 induced apoptosis in a subset of glioma cell lines containing the *mut-p53* gene. We confirmed apoptosis by examining the expression of Annexin V, PARP cleavage, and caspase-7 activation in TAE226-treated glioma cells. We also included two well-characterized wt-p53–containing cell lines (D54 and U343) in the study (25). Results from a quantitative analysis of apoptosis using an Annexin V-FLUOS Apoptosis kit (Roche) are summarized in Fig. 5A. Incubation with 1 μmol/L TAE226 resulted in increased apoptosis in U251 (29%), LN18 (47%), and LN229 (38%) cell lines. However, TAE226 induced only minimal Annexin V–positive staining in the wt-p53–containing cell lines U87, D54, and U343 (<5%). This finding confirmed the cell cycle results, which showed that the U251, LN18, and LN229 cell lines, but not U87 cell line, had a higher sub-G_1 cell population (Fig. 3B). These results strongly correlated p53 status in tumor cells with their sensitivity to TAE226-induced apoptosis. Cleavage of PARP by caspase-3/7 is a hallmark of apoptosis. We examined the expression of PARP cleavage during TAE226-induced apoptosis using Western blot analysis.

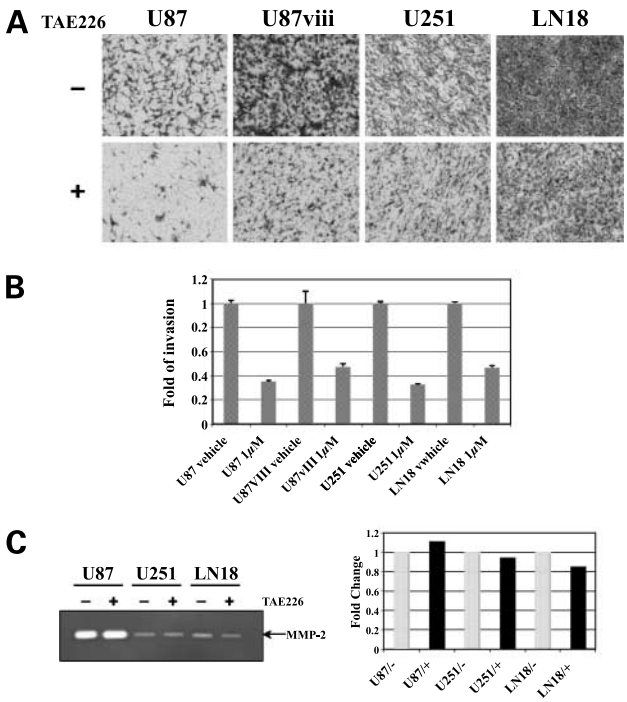

Figure 4. TAE226 treatment inhibits glioma cell invasion. **A,** cells were treated with or without TAE226 for 24 h in serum-containing media before they were trypsinized and counted. Viable cells were resuspended in serum-free media and plated on 8-μm pore size Boyden chambers that were precoated with Matrigel (33 μg per chamber) at 2×10^5 per chamber in a 24-well plate. Invasion assays were done with the indicated cells for 24 h using serum-free media in the lower chamber. *Columns,* mean from three experiments; *bars,* SE. Representative images (×20) of the lower porous membrane surface from Matrigel invasion assays. Crystal violet–stained cells can be distinguished from the 8-μm membrane pores. **B,** effect of TAE226 on tumor invasion was quantified by putting the membranes in 2% deoxycholate for 30 min at room temperature, and absorbance was scored using spectrophotometer with 595-nm wavelength. **C,** gelatin zymographic assay. Cells were treated with 1 μmol/L TAE226 in serum-containing media for 24 h. Media were aspirated and washed 2× with serum-free media. Cells were then cultured in serum-free media for an additional 24 h before collection. Serum-free medium was devoid of cells by centrifugation, and protein concentration was determined. Two micrograms of total protein from serum-free media was subjected to the zymographic analysis. Quantification was done with the ImageJ software, showing that TAE226 did not significantly alter the MMP-2 enzymatic activity.

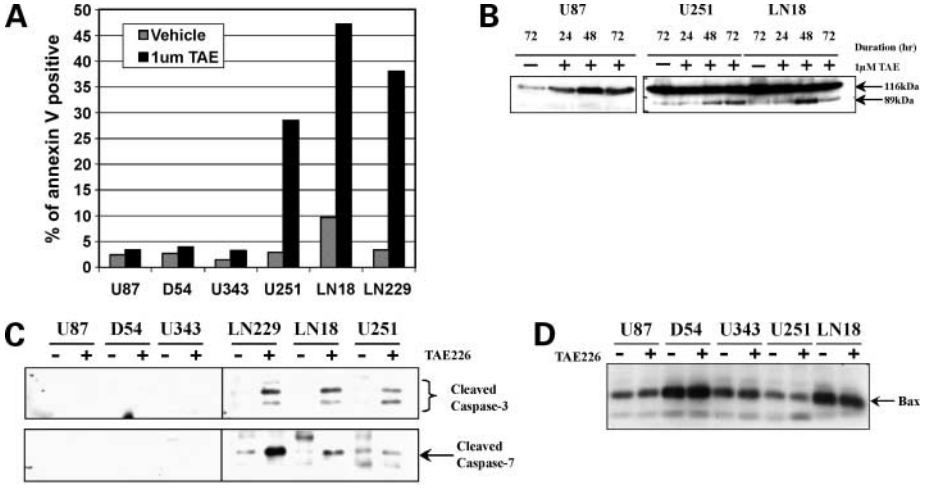

Figure 5. TAE226 treatment induces apoptosis in glioma cells containing mutant p53. **A,** different glioma cell lines were treated with 1 μmol/L TAE226 for 72 h before they were harvested for Annexin V staining as an indication of apoptosis. The population of cells positive for Annexin V staining were compiled as shown. U251, LN18, and LN229 cell lines had a high degree of apoptosis, whereas U87, D54, and U343 cell lines produced minimum Annexin V – positive staining. **B,** glioma cells were treated with 1 μmol/L TAE226 for various time intervals, as indicated. Total protein was extracted and subjected for the detection of PARP cleavage in a Western blotting analysis using an anti-PARP antibody. Results showed that PARP was cleaved after 48 h of TAE226 treatment in U251 and LN18 but not in U87 cells. **C,** caspase-3 and caspase-7 activation was assessed in the protein extracted from cells treated with 1 μmol/L TAE226 for 72 h. Western blotting analysis was done using anti – cleaved caspase-3 or caspase-7 antibodies. Results showed that cleaved caspase-3 bands (17 and 19 kDa) and a cleaved caspase-7 band (20 kDa) were detected only in U251, LN18, and LN229 but not in other wt-p53 – containing glioma cell lines U87, D54, and U343. **D,** Western blotting analysis was also done to detect bax expression. Results showed that bax expression was similar between the untreated and TAE226-treated samples.

After 48 h of exposure to TAE226, an 89-kDa band representing cleaved PARP was readily detectable both in U251 and LN18 cell lines, but not in U87 (Fig. 5B). We examined caspase-3/7 activation in tumor cells after TAE226 treatment. Western blotting analysis was carried out to determine if there was a cleaved caspase-3 and caspase-7 product using an antibody specific for detection of both cleaved caspase-3 (17 and 19 kDa) and caspase-7 (20 kDa), which would serve as an index of its activation. Our results clearly showed that after treatment with TAE226, only mut-p53–containing cell lines, such as U251, LN18, and LN229, showed cleaved caspase-3 and caspase-7 bands but not in TAE-treated wt-p53–containing tumor cell lines (Fig. 5C). The proapoptotic gene *bax* has been shown to be a direct target of p53 (36). As shown in Fig. 5D, TAE226 treatment did not result in induction of bax expression in apoptotic sensitive cell lines such as U251 and LN18. These results established the correlation of p53 status to the sensitivity of TAE226-induced apoptosis and showed that TAE226-induced apoptosis is mediated by caspases, which might be activated by proapoptotic genes other than *bax* in glioma cell lines.

In vivo Effect of TAE226 on Survival of Mice Bearing Intracranial Glioma Xenografts

To assess the potential therapeutic efficacy of TAE226, we did a study to examine the effect of TAE226 treatment on animal survival in an intracranial glioma xenograft model (28). Two glioma cell lines, U87 (wt-p53) and LN229 (mut-p53), were chosen for the study. On day 4 after tumor cell implantation, animals were treated with either vehicle or TAE226 (50 and 75 mg/kg) as described in Materials and Methods. The median survival was 28 and 29 days in vehicle control group for LN229 and U87, respectively (Fig. 6A). Treatment with TAE226 at 50 or 75 mg/kg extended the median survival of U87 xenograft animals by 6 and 7 days, respectively ($P = 0.084$ and $P = 0.042$, respectively, compared with vehicle-treated animals). However, TAE226 treatment of LN229-engrafted animals significantly prolonged their median survival by 19 days (Fig. 6B; $P < 0.004$ for both dosages, compared with vehicle-treated animals). These results not only showed the potential therapeutic efficacy of TAE226 for the treatment of human gliomas but also correlated well with the findings from the *in vitro* studies showing that LN229 cell line was more sensitive to the treatment of TAE226 than U87 cell line.

Discussion

Recent advances in the development of targeted molecular therapies have the advantage of blocking the cell signaling events that govern tumor cell growth, migration, and survival. TAE226 is a potent ATP-competitive inhibitor of several tyrosine protein kinases, including FAK and IGF-IR kinase. We examined the antitumor activity of TAE226 on glioma cells *in vitro*. We found that TAE226 treatment antagonized extracellular matrix–induced autophosphorylation of FAK and IGF-I–induced phosphorylation of IGF-IR, clearly indicating that TAE226 can effectively inhibit its intended targets. It profoundly affected proliferation and invasion of glioma cells. Its ability to inhibit cell cycle progression, particularly at the G_2-M checkpoint, and its effect on inducing apoptosis showed that TAE226 could

potentially be introduced into the clinical setting for the treatment of patients with gliomas.

The expression of FAK and IGF-1R is high, albeit varied among the glioma cell lines tested, suggesting that these kinases are suitable candidates for targeted intervention. The signaling of these two kinases and activity of their downstream target genes was inhibited by TAE226 at concentrations lower than the IC_{50}. It is conceivable that higher concentrations of TAE226 are required to elicit its growth-suppressive effect. Consistent with such a notion, in an effort to assess the effect of TAE226 on cell growth, we found that 1 μmol/L TAE226 can exert >80% reduction of cell viability on day 5 of treatment. Concomitant with the loss of viable cells was the detection of multinucleated and membrane-blebbing cells, suggesting that TAE226 perturbed cell cycle progression and induced programmed cell death. Indeed, cell cycle analysis of TAE226 treatment revealed a high percentage of G_2-M and sub-G_1 populations. The pronounced effect of TAE226 on G_2-M cell cycle arrest was accompanied by a concomitant reduction of the expression of p-cdc2 (Tyr^{15}) and cyclin B1. It has been shown that progression of cells from the G_2 phase of the cell cycle to mitosis (M) is a tightly regulated cellular process that requires cdc2 kinase activation, which precedes the onset of mitosis (37, 38). The activity of cdc2 is regulated in part by the phosphorylation status of the Tyr^{15} residue, which is rapidly dephosphorylated by cdc25 tyrosine phosphatase, triggering entry into mitosis. Decreased expression of p-p34cdc2 (Tyr^{15}), but not total p34cdc2 level by TAE226, may in part force cells to stall at the mitotic phase. The enlarged and multinucleated cells seen in triple immunofluorescence staining assays (Fig. 3C) suggested that several rounds of cell cycle activity occur without mitosis in TAE226-treated cells. Such an observation has been documented previously in that a staurosporine analogue K-252a inhibited p34cdc2 activity, induced G_2-M cell cycle arrest, and produced giant cells containing polyploid nuclei with DNA contents greater than 8N (39). These results also suggested that TAE226 might affect cytokinesis. In contrast to our results, Zhao et al. showed that inhibition of FAK signaling by overexpression of FRNK, a dominant-negative form of FAK, in NIH3T3 cells induced G_1 cell cycle arrest (40). This disparate finding from ours could reflect different cell types and the diverse mechanisms by which TAE226 inactivates FAK activity as well as IGF-IR signaling, whereas FRNK competes with the endogenous FAK in focal contacts for binding signaling molecules such as Src (40).

We also examined how inactivation of FAK and IGF-IR signaling affects glioma invasion in an *in vitro* Matrigel invasion assay. The propensity of glioma cells to invade was reduced to at least 50% of the control, supporting TAE226 anti-invasion activity. The possibility of TAE226 affecting MMP-2 enzymatic activity, thereby inhibiting invasion, was assessed in a gelatin zymographic assay. The result showed that despite inhibiting glioma cell invasion, TAE226 treatment did not significantly affect the MMP-2 enzymatic activity. Invasive tumors possess not only high levels of MMPs but also a high rate of cell motility. Our results suggest that TAE226 inhibition of

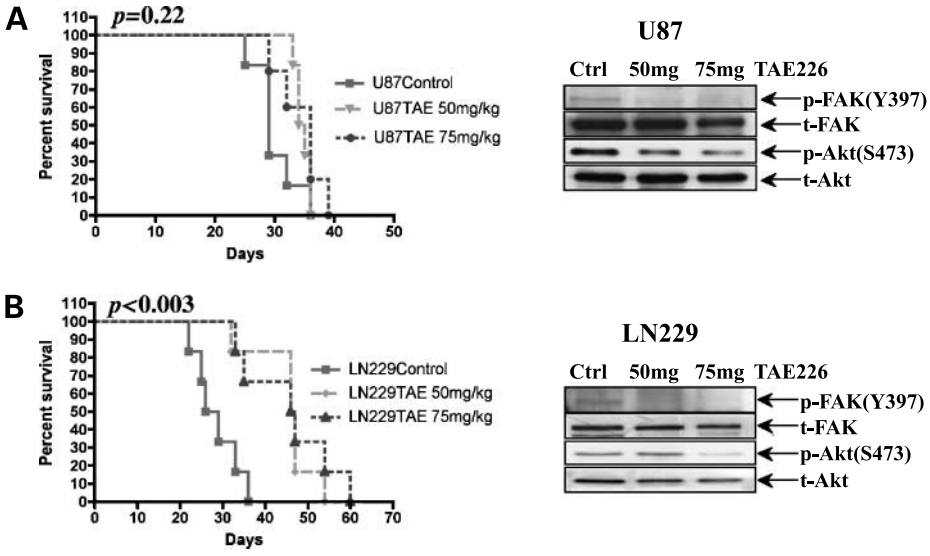

Figure 6. TAE226 treatment prolongs the survival of glioma xenograft animals. **A,** *left,* Kaplan-Meier survival curve for U87 xenograft experiment with *P* of 0.22. *Right,* immunoblotting analyses of both expression and activation of FAK and Akt from tumors following TAE226 treatment. **B,** *left,* Kaplan-Meier survival curve for LN229 xenograft experiment with $P < 0.003$. *Right,* immunoblotting analyses of both expression and activation of FAK and Akt from tumors following TAE226 treatment. The survival curve was plotted from the day of the intracranial implantation of tumor cells (day 0). A total of 18 animals were randomly distributed into three groups that received the following treatments: vehicle control, 50 mg/kg TAE226,75 mg/kg TAE226. The *P* values in the plot determined by the log-rank test represent the comparison of the overall survival of the vehicle-treated mice with that of the TAE226-treated mice. Immunoblotting analyses showed that TAE226 treatment inhibited the activity of both FAK and Akt as assessed by the level of corresponding phospho-protein.

glioma invasion is likely due to its effect on cell motility. However, this assay yielded opposite results to reported findings that overexpression of kinase-dead FAK mutants inhibited tumor metastasis of v-src–transformed cells by suppressing MMP-2 promoter activity, resulting in decreased MMP-2 expression (9). Different experimental system or the abovementioned possibility might contribute to such contradictory findings. It is also possible that TAE226 antagonizes multiple pathways, resulting in different biological outcomes.

Another intriguing finding in this study was that in addition to inducing cell cycle arrest, TAE226 induced apoptosis in a subset of glioma cell lines. This might have been accomplished by the perturbation of IGF-IR signaling resulting from TAE226 treatment. Studies have shown that antagonizing the IGF-IR signaling pathway, either with a kinase-defective IGF-IR (41) or a soluble form of IGF-IR (42), led to apoptosis of tumor cells. Interestingly, the sensitivity of glioma cells to TAE22-induced apoptosis was linked to their p53 status. Those with wt-p53 (e.g., U87, D54, and U343 cell lines) were less sensitive to TAE226-induced apoptosis than cell lines bearing mut-p53 (e.g., U251, LN18, and LN229). Coincidentally, two other studies have also reported a finding of apoptosis induction by different stimuli in a p53-independent manner. First, rapamycin, a mammalian target of rapamycin inhibitor, induced apoptosis in tumor cells lacking functional p53 but not in those with wt-p53 (43). Second, U87 glioma cells were resistant to Adp53-induced apoptosis, in contrast to U251 cells (44). These results strongly suggest that functional p53 protects tumor cells from apoptosis induced by various stimuli. Apoptosis induced by TAE226 clearly progressed through a caspase-dependent pathway, consistent with the detection of cleaved PARP, a substrate of caspase-3 and caspase-7 (45). Several unanswered questions are being scrutinized in continuing experiments regarding the mode of TAE-induced apoptosis. For example, does TAE226 induce apoptosis by activating the mitochondrial (intrinsic) pathway, the death receptor–mediated (extrinsic) pathway, or both pathways? What is the mechanism by which p53 protects tumor cells from TAE226-induced apoptosis? Although we did not detect any change in the level of Bax after TAE226 treatment, we can not exclude the involvement of other proapoptotic and/or antiapoptotic proteins that ultimately alters mitochondria potential leading to caspase activation.

Consistent with the *in vitro* findings of TAE22 exerting a cytotoxic effect on LN229 but cytostatic effect on U87, TAE226 treatment of nude mice bearing LN229 tumor xenografts significantly prolonged animal survival compared with the vehicle-treated animals. On the other hand, TAE226 treatment of U87 xenografts yielded a shorter but statistically significant median survival rate. Although LN229 cell line expressed less FAK and p-FAK than U87, it expressed higher level of IGF-IR than U87. Thus, it is possible that IGF-IR but not FAK signaling weighs more responsibility to the effectiveness of TAE226 treatment both *in vitro* and *in vivo*. Furthermore, our results did not rule out the possibility that inhibition of other pathways may also contribute to the overall cellular sensitivity to TAE226. Taken together, our results show that TAE226 potently suppresses glioma cell growth by disruption of cell cycle progression and/or induction of apoptosis. Simultaneous blockade of the FAK and IGF-IR signaling pathways can potentially be efficacious for treating patients with gliomas upon further development.

Acknowledgments

We thank Bill Sphon for assistance in fluorescence microscopy and Jennifer Edge and Verlene Henry for their excellent effort in performing animal study.

References

1. Jemal A, Thomas A, Murray T, Thun M. Cancer statistics 2002. CA Cancer J Clin 2002;52:23 – 47.

2. Hecker TP, Gladson CL. Focal adhesion kinase in cancer. Front Biosci 2003;8:705 – 14.

3. Gutenberg A, Bruck W, Buchfelder M, Ludwig HC. Expression of tyrosine kinases FAK and Pyk2 in 331 human astrocytomas. Acta Neuropathol 2004;108:224 – 30.

4. Haskell H, Natarajan M, Hecker TP, et al. Focal adhesion kinase is expressed in the angiogenic blood vessels of malignant astrocytic tumors *in vivo* and promotes capillary tube formation of brain microvascular endothelial cells. Clin Cancer Res 2003;9:2157 – 65.

5. Natarajan M, Hecker TP, Gladson CL. FAK signaling in anaplastic astrocytoma and glioblastoma tumors. Cancer J 2003;9:126 – 33.

6. Sieg DJ, Hauck CR, Ilic D, et al. FAK integrates growth-factor and integrin signals to promote cell migration. Nat Cell Biol 2000;2:249 – 56.

7. Parsons JT, Martin KH, Slack JK, Taylor JM, Weed SA. Focal adhesion kinase: a regulator of focal adhesion dynamics and cell movement. Oncogene 2000;19:5606 – 13.

8. McCormack SJ, Brazinski SE, Moore JL, Jr., Werness BA, Goldstein DJ. Activation of the focal adhesion kinase signal transduction pathway in cervical carcinoma cell lines and human genital epithelial cells immortalized with human papillomavirus type 18. Oncogene 1997;15:265 – 74.

9. Hauck CR, Hsia DA, Puente XS, Cheresh DA, Schlaepfer DD. FRNK blocks v-Src-stimulated invasion and experimental metastases without effects on cell motility or growth. EMBO J 2002;21:6289 – 302.

10. Han EK, McGonigal T, Wang J, Giranda VL, Luo Y. Functional analysis of focal adhesion kinase (FAK) reduction by small inhibitory RNAs. Anticancer Res 2004;24:3899 – 905.

11. Del Valle L, Enam S, Lassak A, et al. Insulin-like growth factor I receptor activity in human medulloblastomas. Clin Cancer Res 2002;8:1822 – 30.

12. Antoniades HN, Galanopoulos T, Neville-Golden J, Maxwell M. Expression of insulin-like growth factors I and II and their receptor mRNAs in primary human astrocytomas and meningiomas; *in vivo* studies using *in situ* hybridization and immunocytochemistry. Int J Cancer 1992;50:215 – 22.

13. Scotlandi K, Maini C, Manara MC, et al. Effectiveness of insulin-like growth factor I receptor antisense strategy against Ewing's sarcoma cells. Cancer Gene Ther 2002;9:296 – 307.

14. LeRoith D, Roberts CT, Jr. The insulin-like growth factor system and cancer. Cancer Lett 2003;195:127 – 37.

15. Koda M, Sulkowska M, Kanczuga-Koda L, Sulkowski S. Expression of insulin receptor substrate 1 in primary breast cancer and lymph node metastases. J Clin Pathol 2005;58:645 – 9.

16. Turner BC, Haffty BG, Narayanan L, et al. Insulin-like growth factor-I receptor overexpression mediates cellular radioresistance and local breast cancer recurrence after lumpectomy and radiation. Cancer Res 1997;57:3079 – 83.

17. Nakamura S, Watanabe H, Miura M, Sasaki T. Effect of the insulin-like growth factor I receptor on ionizing radiation-induced cell death in mouse embryo fibroblasts. Exp Cell Res 1997;235:287 – 94.

18. el-Roeiy A, Chen X, Roberts VJ, LeRoith D, Roberts CT, Jr., Yen SS. Expression of insulin-like growth factor-I (IGF-I) and IGF-II and the IGF-I,

IGF-II, and insulin receptor genes and localization of the gene products in the human ovary. J Clin Endocrinol Metab 1993;77:1411 – 8.

19. Resnicoff M, Sell C, Rubini M, et al. Rat glioblastoma cells expressing an antisense RNA to the insulin-like growth factor-1 (IGF-1) receptor are nontumorigenic and induce regression of wild-type tumors. Cancer Res 1994;54:2218 – 22.

20. Pennisi PA, Barr V, Nunez NP, Stannard B, Le Roith D. Reduced expression of insulin-like growth factor I receptors in MCF-7 breast cancer cells leads to a more metastatic phenotype. Cancer Res 2002;62: 6529 – 37.

21. Benini S, Manara MC, Baldini N, et al. Inhibition of insulin-like growth factor I receptor increases the antitumor activity of doxorubicin and vincristine against Ewing's sarcoma cells. Clin Cancer Res 2001;7:1790 – 7.

22. Scotlandi K, Avnet S, Benini S, et al. Expression of an IGF-I receptor dominant negative mutant induces apoptosis, inhibits tumorigenesis and enhances chemosensitivity in Ewing's sarcoma cells. Int J Cancer 2002; 101:11 – 6.

23. Mishima K, Johns TG, Luwor RB, et al. Growth suppression of intracranial xenografted glioblastomas overexpressing mutant epidermal growth factor receptors by systemic administration of monoclonal antibody (mAb) 806, a novel monoclonal antibody directed to the receptor. Cancer Res 2001;61:5349 – 54.

24. Glass TL, Liu TJ, Yung WK. Inhibition of cell growth in human glioblastoma cell lines by farnesyltransferase inhibitor SCH66336. J Neurooncol 2000;2:151 – 8.

25. Ishii N, Maier D, Merlo A, et al. Frequent co-alterations of TP53, p16/ CDKN2A, p14ARF, PTEN tumor suppressor genes in human glioma cell lines. Brain Pathol 1999;9:469 – 79.

26. Cerrato JA, Khan T, Koul D, et al. Differential activation of the Fas/ CD95 pathway by Ad-p53 in human gliomas. Int J Oncol 2004;24:409 – 17.

27. Koul D, Parthasarathy R, Shen R, et al. Suppression of matrix metalloproteinase-2 gene expression and invasion in human glioma cells by MMAC/PTEN. Oncogene 2001;20:6669 – 78.

28. Lal S, Lacroix M, Tofilon P, et al. An implantable guide-screw system for brain tumor studies in small animals. J Neurosurg 2000;92:326 – 33.

29. Abbi S, Guan JL. Focal adhesion kinase: protein interactions and cellular functions. Histol Histopathol 2002;17:1163 – 71.

30. Lopaczynski W, Terry C, Nissley P. Autophosphorylation of the insulin-like growth factor I receptor cytoplasmic domain. Biochem Biophys Res Commun 2000;279:955 – 60.

31. Dimri GP, Lee X, Basile G, et al. A biomarker that identifies senescent human cells in culture and in aging skin *in vivo*. Proc Natl Acad Sci U S A 1995;92:9363 – 7.

32. Serrano M, Lin AW, McCurrach ME, Beach D, Lowe SW. Oncogenic ras provokes premature cell senescence associated with accumulation of p53 and p16INK4a. Cell 1997;88:593 – 602.

33. Fadeel B. Plasma membrane alterations during apoptosis: role in corpse clearance. Antioxid Redox Signal 2004;6:269 – 75.

34. Krek W, Nigg EA. Mutations of p34cdc2 phosphorylation sites induce premature mitotic events in HeLa cells: evidence for a double block to p34cdc2 kinase activation in vertebrates. EMBO J 1991;10:3331 – 41.

35. Yuan J, Yan R, Kramer A, et al. Cyclin B1 depletion inhibits proliferation and induces apoptosis in human tumor cells. Oncogene 2004;23:5843 – 52.

36. Miyashita T, Reed JC. Tumor suppressor p53 is a direct transcriptional activator of the human bax gene. Cell 1995;80:293 – 9.

37. Morgan DO. Principles of CDK regulation. Nature 1995;374:131 – 4.38.

38. Takizawa CG, Morgan DO. Control of mitosis by changes in the subcellular location of cyclin-B1-Cdk1 and Cdc25C. Curr Opin Cell Biol 2000;12:658 – 65.39.

39. Usui T, Yoshida M, Abe K, Osada H, Isono K, Beppu T. Uncoupled cell cycle without mitosis induced by a protein kinase inhibitor, K-252a. J Cell Biol 1991;115:1275 – 82.

40. Zhao JH, Reiske H, Guan JL. Regulation of the cell cycle by focal adhesion kinase. J Cell Biol 1998;143:1997 – 2008.

41. Seely BL, Samimi G, Webster NJ. Retroviral expression of a kinase-defective IGF-I receptor suppresses growth and causes apoptosis of CHO and U87 cells *in-vivo*. BMC Cancer 2002;2:15.

42. D'Ambrosio C, Ferber A, Resnicoff M, Baserga R. A soluble insulin-like growth factor I receptor that induces apoptosis of tumor cells *in vivo* and inhibits tumorigenesis. Cancer Res 1996;56:4013 – 20.

43. Huang S, Shu L, Dilling MB, et al. Sustained activation of the JNK cascade and rapamycin-induced apoptosis are suppressed by p53/ p21(Cip1). Mol Cell 2003;11:1491 – 501.

44. Gomez-Manzano C, Fueyo J, Kyritsis AP, et al. Adenovirus-mediated transfer of the p53 gene produces rapid and generalized death of human glioma cells via apoptosis. Cancer Res 1996;56:694 – 9.

45. D'Amours D, Germain M, Orth K, Dixit VM, Poirier GG. Proteolysis of poly(ADP-ribose) polymerase by caspase 3: kinetics of cleavage of mono(ADP-ribosyl)ated and DNA-bound substrates. Radiat Res 1998; 150:3 – 10.